Nonlinear analysis of efficiency enhancement in free-electron-laser amplifiers

H. P. Freund* and A. K. Ganguly
Naval Research Laboratory, Washington, D.C. 20375
(Received 12 August 1985)

A technique for efficiency enhancement in free-electron-laser and "ubitron" amplifiers (where the ubitron is essentially a free-electron laser operated at electron beam energies less than 500 keV) is analyzed which makes use of both tapered wiggler and axial guide magnetic fields. A set of model equations is derived which describes the coupling between an ensemble of electrons and the radiation field. The analysis is fully three dimensional, and treats the propagation of an electron beam of finite cross-sectional area through a loss-free cylindrical waveguide in the presence of a helically symmetric wiggler field and an axial guide magnetic field. The model equations are solved numerically, and substantial enhancements in the interaction efficiency are found for a variety of choices of the model parameters. The efficiency enhancement is observed to be a sensitive function of both the degree of taper in the wiggler and axial magnetic fields as well as the point at which the taper is begun. In order to illustrate the physical mechanism underlying the efficiency enhancement, a modified pendulum equation which describes the interaction is derived from the orbit equations under a set of idealized assumptions, and used to construct a small-signal theory of the efficiency enhancement.

I. INTRODUCTION

The free-electron laser (FEL) and the "ubitron" have been shown to be feasible radiation sources over a broad spectrum from millimeter through optical wavelengths.[1-12] However, the interaction efficiencies that have been experimentally observed rarely exceed a few percent for systems employing uniform wigglers and axial guide magnetic fields. In order to overcome this problem and achieve significantly higher operating efficiencies, a variety of schemes has been proposed. One approach to efficiency enhancement used in a visible-wavelength FEL experiment using the ACO storage ring at Orsay involves construction of an optical klystron,[8] in which two sections of wiggler magnet are separated by a drift space. In such a device, the first wiggler section and the drift space act to bunch the electron beam in such a way as to enhance the interaction efficiency in the second stage of the wiggler. A more commonly discussed procedure, however, makes use of a tapered wiggler field (in either period or amplitude) to accelerate a bunched electron beam.[13-26] A related approach applicable to FEL or ubitron experiments which employ an axial guide magnetic field involves tapering the axial magnetic field.[27]

The motivation for the present work is to develop a fully-three-dimensional nonlinear analysis and numerical simulation of the FEL or ubitron amplifier with tapered wiggler and axial guide magnetic fields. The analysis we employ is an extension of a previously described nonlinear theory applicable to the case of uniform external fields.[28] The configuration employed consists of an energetic electron beam propagating through a loss-free cylindrical waveguide in the presence of a helically symmetric wiggler and axial guide magnetic field. To this end, a set of coupled nonlinear differential equations is derived which self-consistently describes the evolution of both an ensemble of electrons and the electromagnetic fields. Space-charge fields, however, are neglected and the analysis is valid only in the high-gain Compton regime of operation. The equations are solved numerically for the case in which a monoenergetic electron beam of arbitrary initial cross section is adiabatically injected into the wiggler region. The adiabatic injection is modeled by allowing the wiggler-field amplitude to increase slowly from zero to a constant level. The finite-waveguide geometry is included by the introduction of the boundary conditions appropriate for either the TE or TM modes in a loss-free cylindrical waveguide. Since the configuration of interest is that of a FEL or ubitron amplifier, only single-wave-mode propagation is considered. This permits an average over the wave period to be performed which eliminates the fast-time-scale phenomena from the analysis and results in a great increase in computational efficiency. The effect of magnetic field tapering on the interaction efficiency is greatest only after the bulk of the beam electrons have been trapped (i.e., bunched) in the ponderomotive wave formed by the beating of the wiggler and radiation fields. Hence, we consider a system in which the external magnetic fields are uniform (apart from the initial adiabatic entry taper in the wiggler field) up to a point close to the saturation of the interaction, after which the field tapering is begun. Note that we consider tapers only in the amplitude of the fields (not in the period of the wiggler field) since most operational and proposed experiments employ this approach.

The organization of the paper is as follows. The general equations are presented in Sec. II. In order to illustrate the physical basis for the efficiency enhancement, a modified pendulum equation which describes the axial bunching of the electron beam and a small-signal theory for the gain in the case of tapered wiggler and axial magnetic fields are derived in Sec. III, on the basis of an idealized set of assumptions. Numerical solutions of the general set of coupled nonlinear differential equations are

presented in Sec. IV, and a summary and discussion is given in Sec. V.

II. GENERAL EQUATIONS

The physical configuration we employ includes an axial guide field and helically symmetric wiggler field generated by a bifilar helix, so that the static magnetic field can be written in the form

$$\mathbf{B}(\mathbf{x})=\mathbf{B}_0(z)+\mathbf{B}_w(\mathbf{x}) , \tag{1}$$

where $\mathbf{B}_0(z)$ denotes the axial field,

$$\mathbf{B}_w(\mathbf{x})=2\mathbf{B}_w\left[I_1'(\lambda)\hat{\mathbf{e}}_r\cos\chi-\frac{1}{\lambda}I_1(\lambda)\hat{\mathbf{e}}_\theta\sin\chi+I_1(\lambda)\hat{\mathbf{e}}_z\sin\chi\right] \tag{2}$$

represents the wiggler field in cylindrical coordinates, and $\mathbf{B}_w(z)$ describes the slowly varying amplitude of the wiggler magnetic field. In Eq. (2), $\lambda\equiv k_w r$, $\chi\equiv\theta-k_w z$, $k_w\equiv 2\pi/\lambda_w$ (where λ_w is the wiggler period), and $I_n(\lambda)$ and $I_n'(\lambda)$ represent the modified Bessel function of order n and its derivative, respectively. The adiabatic injection of the electron beam is described by allowing the wiggler amplitude to increase slowly from zero over N_w wiggler periods. In addition, both the wiggler and axial magnetic fields will be tapered starting at some position z_0 close to the saturation point of the interaction. To this end, we choose

$$B_w(z)=\begin{cases}B_w\sin^2(k_w z/4N_w), & 0\le z\le N_w\lambda_w\\ B_w, & N_w\lambda_w\le z\le z_0\\ B_w[1+\epsilon_w k_w(z-z_0)], & z\ge z_0\end{cases} \tag{3}$$

and

$$\mathbf{B}_0(z)=\begin{cases}B_0\hat{\mathbf{e}}_z, & z\le z_0\\ B_0[1+\epsilon_0 k_w(z-z_0)]\hat{\mathbf{e}}_z-\frac{1}{2}B_0\epsilon_0 k_w r\hat{\mathbf{e}}_r, & z\ge z_0\end{cases} \tag{4}$$

where $B_{0,w}$ are constants, and

$$\epsilon_{0,w}\equiv\frac{1}{k_w}\frac{d}{dz}\ln B_{0,w}(z) \tag{5}$$

is assumed to be constant (i.e., to describe a linear taper) for convenience. As a consequence, it will be possible to vary both the degree of taper and the initial point of the taper to determine the optimal configuration. It should be remarked that the representation of the wiggler magnetic field we employ is valid only as long as $\epsilon_w\ll 1$; however, the tapered axial field is self-consistent since it is both curl and divergence free.

Since space-charge fields are neglected in the analysis, the boundary conditions at the waveguide wall may be satisfied by expanding the vector potential in terms of the orthogonal basis functions of the empty guide. Thus, we write the vector potential of the radiation field in the form

$$\delta\mathbf{A}(\mathbf{x},t)=\sum_{\substack{l=0\\n=1}}^{\infty}\delta A_{ln}(z)\left[\frac{l}{k_{ln}r}J_l(k_{ln}r)\hat{\mathbf{e}}_r\sin\alpha_l+J_l'(k_{ln}r)\hat{\mathbf{e}}_\theta\cos\alpha_l\right], \tag{6}$$

for the TE modes, and

$$\delta\mathbf{A}(\mathbf{x},t)=\sum_{\substack{l=0\\n=1}}^{\infty}\delta A_{ln}(z)\left[J_l(k_{ln}r)\hat{\mathbf{e}}_r\cos\alpha_l-\frac{l}{k_{ln}r}J_l(k_{ln}r)\hat{\mathbf{e}}_\theta\sin\alpha_l+\frac{k_{ln}}{k}J_l(k_{ln}r)\hat{\mathbf{e}}_z\sin\alpha_l\right] \tag{7}$$

for the TM modes, where, for frequency ω and wave number $k(z)$,

$$\alpha_l\equiv\int_0^z dz'k(z')+l\theta-\omega t . \tag{8}$$

In Eqs. (6)–(8), J_l and J_l' represent the regular Bessel function of the first kind and its derivative, and k_{ln} describes the cutoff wave number. For the TE modes, $k_{ln}\equiv x_{ln}'/R_g$, where $J_l'(x_{ln}')=0$, and R_g is the waveguide radius. In the case of the TM modes, $k_{ln}\equiv x_{ln}/R_g$, where $J_l(x_{ln})=0$. It is implicitly assumed that both the mode amplitudes $\delta A_{ln}(z)$ and wave number $k(z)$ vary slowly over a wave period.

Substitution of the microscopic fields into Maxwell's equations for the TE mode yields[28]

$$\frac{d^2}{dz^2}\delta a_{ln}+\left[\frac{\omega^2}{c^2}-k^2-k_{ln}^2\right]\delta a_{ln}=\frac{\omega_b^2}{c^2}\beta_{z0}H_{ln}\left\langle\frac{v_1T_l^{(+)}+v_2W_l^{(+)}}{|v_z|}\right\rangle , \tag{9}$$

$$2k^{1/2}\frac{d}{dz}(k^{1/2}\delta a_{ln})=\frac{\omega_b^2}{c^2}\beta_{z0}H_{ln}\left\langle\frac{v_1W_l^{(-)}-v_2T_l^{(-)}}{|v_z|}\right\rangle, \tag{10}$$

where $\delta a_{ln}\equiv e\delta A_{ln}/mc^2$, $\beta_{z0}\equiv v_{z0}/c$, $\omega_b^2\equiv 4\pi e^2 n_b/m$, and (v_1,v_2) are the transverse components of the electron velocity relative to the basis vectors

$$\hat{\mathbf{e}}_1=\hat{\mathbf{e}}_x\cos(k_w z)+\hat{\mathbf{e}}_y\sin(k_w z)$$

and

$$\hat{\mathbf{e}}_2=-\hat{\mathbf{e}}_x\sin(k_w z)+\hat{\mathbf{e}}_y\cos(k_w z) .$$

For the TM modes, we find the similar result

$$\frac{d^2}{dz^2}\delta a_{ln}+\left[1+\frac{k_{ln}^2}{k^2}\right]\left[\frac{\omega^2}{c^2}-k^2-k_{ln}^2\right]\delta a_{ln}=\frac{\omega_b^2}{c^2}\beta_{z0}H_{ln}\left\langle\frac{v_1T_l^{(+)}+v_2W_l^{(+)}+2(k_{ln}/k)v_zJ_l(k_{ln}r)\sin\alpha_l}{|v_z|}\right\rangle, \tag{11}$$

and

$$2\left[k+\frac{k_{ln}^2}{k}\right]^{1/2}\frac{d}{dz}\left[\left[k+\frac{k_{ln}^2}{k}\right]^{1/2}\delta a_{ln}\right]=\frac{\omega_b^2}{c^2}\beta_{z0}H_{ln}\left\langle\frac{v_1W_1^{(-)}-v_2T_l^{(-)}+2(k_{ln}/k)v_zJ_l(k_{ln}r)\cos\alpha_l}{|v_z|}\right\rangle. \tag{12}$$

In the preceding equations, H_{ln}, $T_l^{(\pm)}$, and $W_l^{(\pm)}$ are mode- (i.e., polarization-) dependent quantities defined as

$$H_{ln}=\begin{cases}\dfrac{(x'_{ln})^2}{[(x'_{ln})^2-l^2]J_l^2(x'_{ln})}, & \mathrm{TE}_{ln}\text{ mode}\\ \dfrac{1}{[J'_l(x_{ln})]^2}, & \mathrm{TM}_{ln}\text{ mode}\end{cases} \tag{13}$$

and

$$T_l^{(\pm)}\equiv\begin{cases}F_l^{(\pm)}\sin\psi_l+G_l^{(\pm)}\cos\psi_l, & \mathrm{TE}_{ln}\text{ mode}\\ F_l^{(\mp)}\cos\psi_l-G_l^{(\mp)}\sin\psi_l, & \mathrm{TM}_{ln}\text{ mode}\end{cases} \tag{14}$$

$$W_l^{(\pm)}\equiv\begin{cases}F_l^{(\mp)}\cos\psi_l-G_l^{(\mp)}\sin\psi_l, & \mathrm{TE}_{ln}\text{ mode}\\ -(F_l^{(\pm)}\sin\psi_l+G_l^{(\pm)}\cos\psi_l), & \mathrm{TM}_{ln}\text{ mode}\end{cases} \tag{15}$$

where

$$\psi_l\equiv\psi_0+\int_0^z dz'\left[k+lk_w-\frac{\omega}{v_z}\right] \tag{16}$$

is the phase relative to the ponderomotive frame, ψ_0 ($\equiv-\omega t_0$) is the initial phase,

$$F_l^{(\pm)}\equiv J_{l-1}(k_{ln}r)\cos[(l-1)\chi]\pm J_{l+1}(k_{ln}r)\cos[(l+1)\chi], \tag{17}$$

and

$$G_l^{(\pm)}\equiv J_{l-1}(k_{ln}r)\sin[(l-1)\chi]\pm J_{l+1}(k_{ln}r)\sin[(l+1)\chi]. \tag{18}$$

Finally,

$$\langle F\rangle\equiv\frac{1}{2\pi^2R_g^2}\int_{-\pi}^{\pi}d\psi_0\sigma_{||}(\psi_0)\int_{A_g}\int d\theta_0dr_0r_0\sigma_\perp(r_0,\theta_0)F \tag{19}$$

describes the average of the beam electrons over both the initial axial phase and cross section of the waveguide. It is important to recognize that this average includes the effect of the overlap of the electron beam with the transverse-mode structure of the radiation field (often included in one-dimensional formulations in an *ad hoc* manner by the inclusion of a filling factor) in a self-consistent way.

In order to complete the formulation, the electron-orbit equations in the presence of the static and fluctuation fields must be specified. Since we describe an amplifier configuration, we choose to integrate in z and write the Lorentz force equation in the form

$$v_z\frac{d}{dz}\mathbf{p}=-e\delta\mathbf{E}_{ln}-\frac{e}{c}\mathbf{v}\times(\mathbf{B}_0+\mathbf{B}_w+\delta\mathbf{B}_{ln}), \tag{20}$$

where

$$\delta\mathbf{E}_{ln}=-\frac{1}{c}\frac{\partial}{\partial t}\delta\mathbf{A}_{ln},\quad \delta\mathbf{B}_{ln}=\nabla\times\delta\mathbf{A}_{ln} \tag{21}$$

are evaluated using the appropriate expressions for $\delta\mathbf{A}_{ln}$ for either the TE_{ln} or TM_{ln} mode.

The interested reader is referred to Ganguly and Freund[28] for a more detailed description of the derivation of the dynamical equations.

III. THE SMALL-SIGNAL THEORY

In order to illustrate the underlying mechanism for the efficiency enhancement of a tapered field configuration, we derive a modified pendulum equation for the axial phase ψ_l which describes the phase trapping of the electron beam in the ponderomotive potential formed by the beating of the wiggler and radiation fields. For convenience, we consider only the TE mode.

The orbit equations for the TE_{ln} mode (20) are of the form

$$\gamma\frac{d}{dt}v_1=-\{\Omega_0[1+\epsilon_0k_w(z-z_0)]-\gamma k_wv_3+2\Omega_w(z)I_1(\lambda)\sin\chi\}v_2+\Omega_w(z)v_3I_2(\lambda)\sin(2\chi)-\tfrac{1}{2}\Omega_0v_3\epsilon_0\lambda\sin\chi$$
$$-\tfrac{1}{2}c\delta a_{ln}\left\{\left[\omega\left[1-\frac{v_1^2}{c^2}\right]-kv_3\right]W_l^{(-)}-2k_{ln}v_2J_l(k_{ln}r)\cos\alpha_l+\frac{v_1v_2}{c^2}\omega T_l^{(+)}\right\}, \tag{22}$$

$$\gamma\frac{d}{dt}v_2=\{\Omega_0[1+\epsilon_0k_w(z-z_0)]-\gamma k_wv_3+2\Omega_w(z)I_1(\lambda)\sin\chi\}v_1-\Omega_w(z)v_3[I_0(\lambda)+I_2(\lambda)\cos(2\chi)]+\tfrac{1}{2}\Omega_0v_3\epsilon_0\lambda\cos\chi$$
$$+\tfrac{1}{2}c\delta a_{ln}\left\{\left[\omega\left[1-\frac{v_2^2}{c^2}\right]-kv_3\right]T_l^{(+)}-2k_{ln}v_1J_l(k_{ln}r)\cos\alpha_l+\frac{v_1v_2}{c^2}\omega W_l^{(-)}\right\}, \tag{23}$$

$$\gamma\frac{d}{dt}v_3=\Omega_w(z)v_2[I_0(\lambda)+I_2(\lambda)\cos(2\chi)]-\Omega_w(z)v_1I_2(\lambda)\sin(2\chi)+\tfrac{1}{2}\Omega_0\epsilon_0\lambda(v_1\sin\chi-v_2\cos\chi)$$
$$-\tfrac{1}{2}c\delta a_{ln}\left[k-\omega\frac{v_3}{c^2}\right](v_1W_l^{(-)}-v_2T_l^{(+)}) , \tag{24}$$

$$\frac{d}{dt}\gamma=-\frac{1}{2}\frac{\omega}{c}\delta a_{ln}(v_1W_l^{(-)}-v_2T_l^{(+)}) , \tag{25}$$

$$\frac{d}{dt}\chi=k_w\lambda^{-1}(-v_1\sin\chi+v_2\cos\chi-\lambda v_3) , \tag{26}$$

$$\frac{d}{dt}\lambda=k_w(v_1\cos\chi+v_2\sin\chi) , \tag{27}$$

and

$$\frac{d}{dt}\psi_l=(k+lk_w)v_3-\omega , \tag{28}$$

where

$$\Omega_w(z)\equiv\Omega_w+\delta\Omega_w(z) ,$$

$$\Omega_{0,w}\equiv|eB_{0,w}/mc| ,$$

and

$$\delta\Omega_w(z)\equiv\Omega_w\epsilon_wk_w(z-z_0) . \tag{29}$$

Solution of these equations will be found under the assumption that terms in $\epsilon_{0,w}$ and δa_{ln} are all of first order, and a perturbation theory about the zeroth-order solutions will be derived.

A class of zeroth-order, steady-state solutions has been extensively discussed in the literature,[29–32] and are characterized by $\mathbf{v}_0=v_w\hat{\mathbf{e}}_1+v_{||}\hat{\mathbf{e}}_z$, $\chi_0=\pm\pi/2$, and $\lambda_0=\mp v_w/v_{||}$, where

$$v_w=\frac{2\Omega_wv_{||}I_1(\lambda_0)/\lambda_0}{\Omega_0-\gamma k_wv_{||}\pm2\Omega_wI_1(\lambda_0)} . \tag{30}$$

Closure of these equations is found by noting that

$$v_w^2+v_{||}^2=(1-\gamma_0^{-2})c^2 . \tag{31}$$

Note that two distinct classes of trajectories are found corresponding to relatively low axial guide fields (upper sign) for which $\Omega_0<\gamma_0k_wv_{||}$, and relatively high axial guide fields (lower sign) for $\Omega_0>\gamma_0k_wv_{||}$. For convenience, we shall refer to the trajectories corresponding to low axial guide fields as group I, and those for high axial fields as group II. Perturbing about these steady-state orbits, we write $v=v_0+\delta v$, $\chi=\chi_0+\delta\chi$, $\lambda=\lambda_0+\delta\lambda$, $\gamma=\gamma_0+\delta\gamma$, and obtain to first order

$$\gamma_0\delta\dot{v}_1=-[\Omega_0-\gamma_0k_wv_{||}\pm2\Omega_wI_1(\lambda_0)]\delta v_2-2\Omega_wI_2(\lambda_0)\delta\chi-\frac{c}{2}\delta a_{ln}\left[\omega\left[1-\frac{v_w^2}{c^2}\right]-k_wv_{||}\right]W_l^{(-)} , \tag{32}$$

$$\gamma_0\delta\dot{v}_2=[\Omega_0-\gamma_0k_wv_{||}\pm2\Omega_wI_1(\lambda_0)]\delta v_1-\frac{v_w}{v_{||}}[\Omega_0\pm2\Omega_wI_1(\lambda_0)]\delta v_3$$
$$-k_wv_wv_{||}\delta\gamma-2\Omega_wv_{||}\frac{\delta\lambda}{\lambda_0}[I_2(\lambda_0)+\lambda_0^2I_0(\lambda_0)-\lambda_0I_1(\lambda_0)]$$
$$+v_w\Omega_0\epsilon_0k_w(z-z_0)-2v_{||}\left[\frac{1+\lambda_0^2}{\lambda_0}\right]I_1(\lambda_0)\delta\Omega_w$$
$$+\frac{c}{2}\delta a_{ln}[(\omega-kv_{||})T_l^{(+)}-2k_{ln}v_wJ_l(k_{ln}R_0)\cos\alpha_l] , \tag{33}$$

$$\gamma_0\delta\dot{v}_3=2\Omega_w\frac{1}{\lambda_0}I_1(\lambda_0)\delta v_2+2\Omega_wv_wI_2(\lambda_0)\delta\chi-\frac{c}{2}\delta a_{ln}v_w\left[k-\omega\frac{v_{||}}{c^2}\right]W_l^{(-)} , \tag{34}$$

$$\delta\dot{\gamma}=-\tfrac{1}{2}\delta a_{ln}\omega\frac{v_w}{c}W_l^{(-)} , \tag{35}$$

$$\delta\dot{\chi}=-k_w\left[\delta v_3\pm\frac{1}{\lambda_0}\delta v_1\mp\frac{1}{\lambda_0^2}v_w\delta\lambda\right] , \tag{36}$$

and

$$\delta\dot{\lambda}=\pm k_w(\delta v_2-v_w\delta\chi) , \tag{37}$$

where $R_0\equiv\lambda_0/k_w$. Observe that to this order

$$T_l^{(+)} \simeq 2J_l'(k_{ln}R_0)\sin[\psi_l+(l-1)\chi_0] , \tag{38}$$

and

$$W_l^{(-)} \simeq 2J_l'(k_{ln}R_0)\cos[\psi_l+(l-1)\chi_0] . \tag{39}$$

We have implicitly assumed that $\lambda_0 < 1$ in the perturbation analysis, so that the contribution from the radial component of $\mathbf{B}_0$ can be ignored.

Differentiating Eqs. (33) and (36) with respect to time, we obtain

$$\left[\frac{d^2}{dt^2}+\omega_1^2\right]\delta\chi = \frac{1}{c}A_2\delta v_2 - \frac{1}{\gamma_0}\delta a_{ln}A_1\cos[\psi_l+(l-1)\chi_0] \tag{40}$$

and

$$\left[\frac{d^2}{dt^2}+\omega_2^2\right]\delta v_2 = cB_2\delta\chi + \frac{1}{\gamma_0}k_w v_w v_{||}[\epsilon_0\Omega_0-\epsilon_w(\Omega_0-\gamma_0 k_w v_{||})] - \frac{c}{\gamma_0}\delta a_{ln}B_1\cos[\psi_l+(l-1)\chi_0] , \tag{41}$$

where

$$\omega_1^2 \equiv k_w^2 v_{||}^2 \mp \frac{2}{\gamma_0}\Omega_w k_w v_{||}\left[\frac{1+\lambda_0^2}{\lambda_0}\right]I_2(\lambda_0) , \tag{42}$$

$$\omega_2^2 \equiv \frac{1}{\gamma_0^2}(\Omega_0-\gamma_0 k_w v_{||})[\Omega_0-\gamma_0 k_w v_{||}\pm 2\Omega_w I_1(\lambda_0)] \pm \frac{2}{\gamma_0}\Omega_w k_w v_{||}\left[\frac{1+\gamma_0^2}{\lambda_0}\right]I_2(\lambda_0) , \tag{43}$$

$$A_2 \equiv \pm\frac{ck_w}{\gamma_0\lambda_0}(\Omega_0-2\gamma_0 k_w v_{||}) \tag{44}$$

$$B_2 \equiv -\frac{2}{\gamma_0^2}\Omega_w\frac{v_{||}}{c}\left[(1+\lambda_0^2)[\Omega_0\pm 2\Omega_w I_1(\lambda_0)]I_2(\lambda_0)+\gamma_0\lambda_0^2 k_w v_{||}\left[I_0(\lambda_0)-\frac{1}{\lambda_0}I_1(\lambda_0)\right]\right] , \tag{45}$$

$$A_1 \equiv \mp\frac{ck_w}{\gamma_0\lambda_0}[\omega-kv_{||}(1+\lambda_0^2)]J_l'(k_{ln}R_0) , \tag{46}$$

$$B_1 = \frac{1}{\gamma_0}\{[\omega-kv_{||}(1+\lambda_0^2)][\Omega_0\pm 2\Omega_w I_1(\lambda_0)]-\gamma_0 k_w v_{||}(\omega-kv_{||})\}J_l'(k_{ln}R_0) + \Delta\omega_l\left[\frac{l}{k_{ln}r_0}(\omega-kv_{||})\pm k_{ln}v_w\right]J_l(k_{ln}R_0) , \tag{47}$$

and $\Delta\omega_l \equiv \omega-(k+lk_w)v_{||}$. This pair of coupled second-order differential equations can be converted into the following set of two uncoupled fourth-order differential equations:

$$\left[\frac{d^2}{dt^2}+\Omega_1^2\right]\left[\frac{d^2}{dt^2}+\Omega_2^2\right]\delta v_2 = \frac{1}{\gamma_0}k_w v_w v_{||}\omega_1^2[\epsilon_0\Omega_0-\epsilon_w(\Omega_0-\gamma_0 k_w v_{||})] - \frac{c}{\gamma_0}\delta a_{ln}[(\omega_1^2-\Delta\omega_l^2)B_1+A_1B_2]\cos[\psi_l+(l-1)\chi_0] \tag{48}$$

and

$$\left[\frac{d^2}{dt^2}+\Omega_1^2\right]\left[\frac{d^2}{dt^2}+\Omega_2^2\right]\delta\chi = \frac{1}{\gamma_0}k_w v_w\frac{v_{||}}{c}A_2[\epsilon_0\Omega_0-\epsilon_w(\Omega_0-\gamma_0 k_w v_{||})] - \frac{1}{\gamma_0}\delta a_{ln}[(\omega_2^2-\Delta\omega_l^2)A_1+A_2B_1]\cos[\psi_l+(l-1)\chi_0] , \tag{49}$$

where

$$\Omega_{1,2}^2 \equiv \tfrac{1}{2}(\omega_1^2+\omega_2^2)\pm\tfrac{1}{2}[(\omega_1^2-\omega_2^2)^2+4A_2B_2]^{1/2} . \tag{50}$$

If we now assume that the FEL or ubitron resonance condition is satisfied, that is, $\dot{\psi}_l \simeq \Delta\omega_l \simeq 0$, then operating on the $\delta\dot{v}_3$ equation (34) with the fourth-order differential operators in Eqs. (48) and (49) can be shown to give

$$\frac{d}{dt}\delta v_3 = \frac{k_w v_{||}^2}{\gamma_{||}^2}\frac{1-\Phi(\lambda_0)}{\gamma_0 k_w v_{||} \pm 2\Omega_w \lambda_0^{-1} Z(\lambda_0)}[\epsilon_0\Omega_0 - \epsilon_w(\Omega_0 - \gamma_0 k_w v_{||})] - \frac{c v_w (k+lk_w)}{\gamma_0 \gamma_{||}^2}\delta a_{ln}\Phi(\lambda_0) J_l'(k_{ln}R_0)\cos[\psi_l + (l-1)\chi_0] , \tag{51}$$

where

$$\Phi(\lambda_0) \equiv 1 + \frac{\gamma_{||}^2 \lambda_0 I_1(\lambda_0)[\gamma_0 k_w v_{||} \pm 2\Omega_w \lambda_0^{-1} Z(\lambda_0)]}{\{(1+\lambda_0^2)[\Omega_0 \pm 2\Omega_w I_1(\lambda_0)] - \gamma_0 k_w v_{||}\} Z(\lambda_0) - \lambda_0^2 \gamma_0 k_w v_{||} Y(\lambda_0)} , \tag{52}$$

$$Z(\lambda_0) \equiv (1+\lambda_0^2) I_1'(\lambda_0) - \frac{2}{\lambda_0} I_l(\lambda_0) , \tag{53}$$

and

$$Y(\lambda_0) \equiv (1+\lambda_0^2) I_1'(\lambda_0) - \frac{1}{\gamma_0} I_1(\lambda_0) . \tag{54}$$

The modified pendulum equation follows immediately by noting that

$$\frac{d}{dt}\delta v_3 = \frac{v_{||}^3}{\omega}\frac{d^2}{dz^2}\psi_l , \tag{55}$$

so that we obtain

$$\frac{d^2}{dz^2}\psi_l = -K_l^2\{\cos[\psi_l + (l-1)\chi_0] - \cos[\psi_{\rm res} + (l-1)\chi_0]\} , \tag{56}$$

where

$$K_l^2 \equiv \frac{c v_w (k+lk_w)^2}{\gamma_0 \gamma_{||}^2 v_{||}^2}\delta a_{ln}\Phi(\lambda_0) J_l'(k_{ln}R_0) , \tag{57}$$

and the resonant phase $\psi_{\rm res}$ is given by

$$\cos[\psi_{\rm res} + (l-1)\chi_0] \equiv \mp \frac{\gamma_0 k_w v_{||}}{\gamma_0 k_w v_{||} \pm 2\Omega_w \lambda_0^{-1} Z(\lambda_0)}\frac{1-\Phi(\lambda_0)}{\lambda_0 \Phi(\lambda_0)}\frac{\beta_{||}}{\delta a_{ln} J_l'(k_{ln}R_0)}\frac{\Omega_0\epsilon_0 - \epsilon_w(\Omega_0 - \gamma_0 k_w v_{||})}{\omega} \tag{58}$$

for $\beta_{||} = v_{||}/c$.

In order to illustrate the implications of this expression for the resonant phase (58) for the efficiency enhancement in a tapered system, we now consider the small-signal gain. We observe that the zeroth-order steady-state orbits describe helical trajectories and assume that the configuration of the electron beam is that of a "thin" helix of radius ΔR centered about the position of the steady-state orbit. Hence, we take $\sigma_\perp(r_0,\theta_0) = \pi \Delta R^2 \delta(\theta_0 - \chi_0)\delta(r_0 - R_0)/r_0$. It then follows from Eq. (10) that

$$k^{1/2}\frac{d}{dz}(k^{1/2}\delta a_{ln}) \simeq \mp \frac{\omega_b^2}{c^2}\beta_{z0}(k_{ln}\Delta R)^2 \frac{\lambda_0 J_l'(k_{ln}R_0)}{(x_{ln}'^2 - l^2) J_l^2(x_{ln}')}\langle \cos[\psi_l + (l-1)\chi_0]\rangle_{\psi_0} , \tag{59}$$

where the average is now purely over the initial phase ψ_0. For a beam sufficiently tenuous that the gain is small, we assume that the wave vector is constant and given approximately by

$$k^2 = \frac{\omega^2}{c^2} - k_{ln}^2 . \tag{60}$$

We assume the system has run to saturation at $z = z_0$, at which point the electrons have been trapped by the ponderomotive potential, and define the gain over a length L relative to z_0 as

$$G_L \equiv \frac{\delta a_{ln}(z = L + z_0) - \delta a_{ln}(z = z_0)}{\delta a_{ln}(z = z_0)} , \tag{61}$$

subject to the requirement that $G_L < 1$. It can be shown from (59) that

$$G_L \simeq \mp \frac{\omega_b^2}{c^2 k_w^2}\frac{\beta_{z0}}{\delta a_{ln}}(k_{ln}\Delta R)^2 \frac{\lambda_0 J_l'(k_{ln}R_0)}{(x_{ln}'^2 - l^2) J_l^2(x_{ln}')}\frac{k_w^2}{k}\int_{z_0}^{L+z_0} dz \langle \cos[\psi_l + (l-1)\chi_0]\rangle_{\psi_0} . \tag{62}$$

In the trapped-particle regime $\psi_l \simeq \psi_{\rm res}$, and the gain can be expressed as

$$G_L \simeq \frac{\omega_b^2}{c^2 k_w^2}\frac{\beta_{||}^2}{\delta a_{ln}^2}\frac{L k_w^2}{\omega k}\frac{(k_{ln}\Delta R)^2}{(x_{ln}'^2 - l^2) J_l^2(x_{ln}')}\frac{\gamma_0 k_w v_{||}}{\gamma_0 k_w v_{||} \pm 2\Omega_w \lambda_0^{-1} Z(\lambda_0)}\frac{1-\Phi(\lambda_0)}{\Phi(\lambda_0)}[\epsilon_0\Omega_0 - \epsilon_w(\Omega_0 - \gamma_0 k_w v_{||})] , \tag{63}$$

using Eq. (58). The gain in the tapered field region, therefore, depends upon the resonant phase and is proportional to the slopes of the tapered fields. Note that the total gain relative to the start of the interaction region ($z=0$) is the sum of the gains for the uniform and tapered field regions.

The essential feature of the efficiency enhancement mechanism which this idealized theory illustrates is the effect of the axial guide field on the sense in which the fields must be tapered to provide for an enhancement. In order to show this, we must first describe some characteristics of the steady-state trajectories. The axial velocity and $\Phi(\lambda_0)$ are plotted in Figs. 1 and 2 as functions of the axial guide field for an arbitrary choice of parameters. Note that the dashed line in Fig. 1 corresponds to orbitally unstable trajectories, and $\Phi(\lambda_0)$ calculated in Fig. 2 corresponds to the stable orbits. For our present purposes we are most interested in the behavior of $\Phi(\lambda_0)$, and we observe that $\Phi(\lambda_0)$ displays singularities corresponding to the transitions to orbital instability for both group-I and group-II orbits. It is also evident from Fig. 2 that $\Phi(\lambda_0)>1$ over the entire range of stable group-I orbits, while $\Phi(\lambda_0)<1$ for group-II trajectories. Indeed, $\Phi(\lambda_0)<0$, corresponding to group-II orbits with $B_0\simeq 14.2$ kG for the chosen parameters.

In view of these characteristics of the steady-state orbits, it follows from the expressions for G_L, (63), that both the axial and wiggler fields must be tapered "down" (i.e., $\epsilon_0<0$ and $\epsilon_w<0$) to achieve an enancement in the gain and efficiency for group-I orbit parameters ($\Omega_0<\gamma_0 k_w v_{||}$). However, the situation is more complicated in the case of group-II orbits ($\Omega_0>\gamma_0 k_w v_{||}$), for which two distinct regimes occur. When $0<\Phi(\lambda_0)<1$, the axial field must be tapered "up" (i.e., $\epsilon_0>0$), while the wiggler field must be tapered "down" ($\epsilon_w<0$) to achieve an efficiency enhancement. In contrast, when $\Phi(\lambda_0)<0$ efficiency enhancement occurs when either the axial field is tapered "down" or the wiggler field is tapered "up."

In order to understand this behavior we note that the characteristics of the zeroth-order, steady-state orbits imply that

$$dv_{||}/d\gamma \sim \Phi, \quad dv_{||}/dB_0 \sim (1-\Phi),$$

and

$$dv_{||}/dB_w \sim (\Phi-1)(\Omega_0-\gamma_0 k_w v_{||}).$$

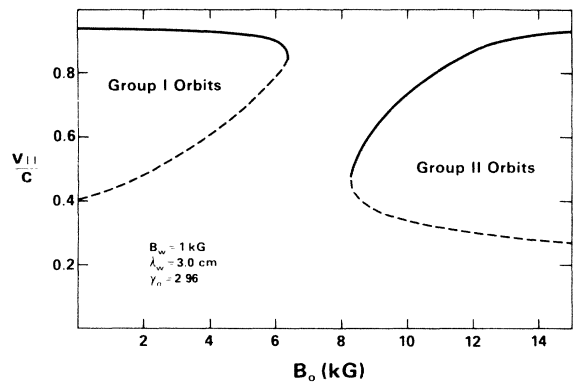

FIG. 1. Plot of the axial velocity vs axial guide field for the ideal steady-state orbits.

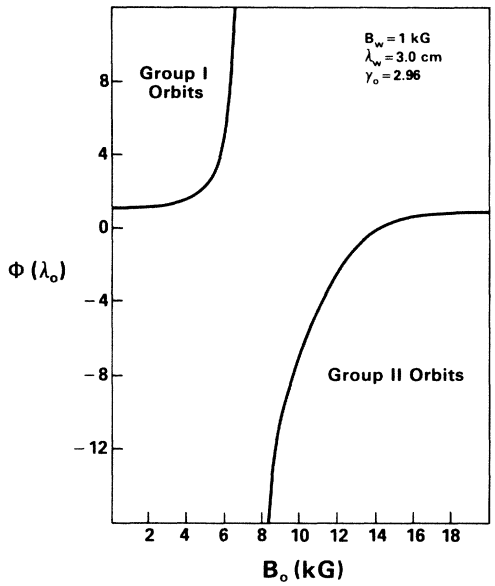

FIG. 2. Plot of $\Phi(\lambda_0)$ corresponding to the stable steady-state trajectories.

For group-I orbit parameters, therefore, the electrons are axially decelerated as they lose energy to the radiation field, and must be accelerated through the effect of the tapered fields to maintain resonance. Since $\Phi(\lambda_0)>1$ and $\Omega_0<\gamma_0 k_w v_{||}$ for group-I orbits, this is accomplished by decreasing both the axial and wiggler fields. A similar situation holds for group-II orbits when $0<\Phi(\lambda_0)<1$, except that the axial acceleration of the electrons is accomplished by means of increasing the axial field and decreasing the wiggler field. However, when $\Phi(\lambda_0)<0$ for group-II orbits, the electrons are axially accelerated as energy is lost to the radiation field. This "negative-mass" type of effect is accompanied by an enhanced energy loss in the transverse velocity. As a result, the electrons must be decelerated by the tapering of the external fields in order to maintain resonance with the wave. This is accomplished by decreasing the axial field and increasing the wiggler field. These conclusions formed on the basis of an idealized small-signal theory are fully borne out by the simulation results described in the next section, for which no such ideal assumptions are imposed.

It should be remarked that the FEL or ubitron mechanism is extremely sensitive to the presence of an initial spread in the axial momentum (or velocity) spread of the electron beam. This occurs because the effect of the initial velocity spread is to render the particle-trapping mechanism ineffective and, while resonant amplification of the radiation field may still occur, the nonlinear efficiency of the interaction is substantially reduced. Since the tapered field efficiency enhancement scheme described herein involves the acceleration or deceleration of electrons which have been trapped by the ponderomotive wave formed by the beating of the wiggler and radiation fields, the presence of an initial beam-velocity spread also renders the efficiency enhancement process ineffective.

In order to determine some measure for the maximum allowable-velocity spread, we consider the nonlinear pen-

dulum equation (56) which describes electron motion in the ponderomotive potential. In the uniform field region $\cos[\psi_{res}+(l-1)\chi_0]=0$, and the equation can be integrated to give

$$\left[\frac{d}{dz}\psi_l\right]^2=-2K_l^2\sin[\psi_l+(l-1)\chi_0]+C\ , \tag{64}$$

where C is an integration constant. The separatrices between trapped and untrapped trajectories are given by

$$\frac{d}{dz}\psi_l=2\,|\,K_l\,|\left[\frac{1-\sin[\psi_l+(l-1)\chi_0]}{2}\right]^{1/2}, \tag{65}$$

when $v_w\Phi(\lambda_0)>0$, and

$$\frac{d}{dz}\psi_l=2\,|\,K_l\,|\left[\frac{1+\sin[\psi_l+(l-1)\chi_0]}{2}\right]^{1/2} \tag{66}$$

when $v_w\Phi(\lambda_0)<0$. The depth of the separatrix (i.e., the trapping potential), therefore, is $4\,|\,K_l\,|$. Since

$$\frac{d\psi_l}{dz}=k+lk_w-\omega/v_z\ ,$$

this corresponds to an axial velocity spread of

$$\frac{\Delta v_{||}}{v_{||}}=\frac{4\,|\,K_l\,|\,v_{||}}{\omega}\ . \tag{67}$$

In order for the particle-trapping mechanism to be effective, the initial velocity spread must be much less than the effective velocity spread (67) associated with the trapped particle trajectories at saturation. Thus, we write

$$\left[\frac{\Delta v_z}{v_z}\right]_{z=0}\ll 4\left[\frac{cv_w}{\gamma_0\gamma_{||}^2v_{||}^2}\delta a_{ln}\,|\,\Phi(\lambda_0)\,|\,J_l'(k_{ln}R_0)\right]^{1/2}, \tag{68}$$

where δa_{ln} is to be evaluated at saturation.

For the parameters associated with the various cases considered in this work, it follows that $(\Delta v_z/v_z)_{z=0}$ must be less than a few percent. However, it is important to consider the effect of the axial guide field on this constraint. As shown in the preceding discussion, v_w and $\Phi(\lambda_0)$ are both enhanced near the resonance at $\Omega_0\sim\gamma_0k_wv_{||}$ relative to the zero-guide-field limit, and $v_{||}$ is decreased. In addition, it has been shown that the saturation efficiency may also be enhanced,[33] leading to an increase in δa_{ln} at saturation for $\Omega_0\sim\gamma_0k_wv_{||}$ as well. The effect of this is to increase resonantly the depth of the trapping potential near resonance, which permits operation for somewhat greater levels of the initial velocity spread.

IV. NUMERICAL SIMULATION

The set of coupled nonlinear differential equations described in Sec. II is solved numerically for a configuration in which the initial state is chosen to model the injection of a solid, axisymmetric, monoenergetic electron beam of zero emittance and uniform cross section. Hence, we choose $\sigma_\perp=\sigma_{||}=1$, and initially set $\mathbf{p}_\perp=0$ and $p_{||}=mc(\gamma_0^2-1)^{1/2}$. The averages in Eqs. (9)–(12) are performed by means of an Nth-order Gaussian quadrature technique in each of the variables (ψ_0,r_0,θ_0); hence, the total number of particles included in the simulation is N^3. For all the cases discussed herein, a choice of $N=10$ was found to provide an accuracy of better than 0.1%. The initial electron positions are chosen by means of the Gaussian algorithm within the ranges $-\pi\le\psi_0\le\pi$, $0\le\theta_0\le2\pi$, and $0\le r_0\le R_b$. A more detailed description of the numerical procedure is given in Ganguly and Freund.[28]

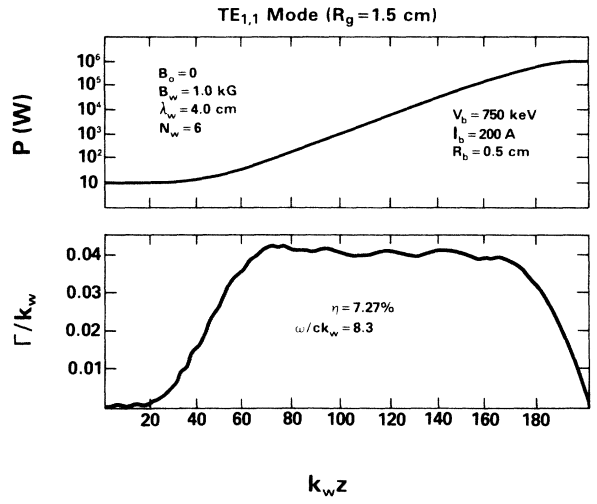

FIG. 3. Graphs of the radiation power and growth rate vs axial position for a $TE_{1,1}$ mode and in the absence of an axial guide field.

The first case we consider treats model parameters in the absence of an axial guide field ($B_0=0$). The wiggler field is characterized by $B_w=1.0$ kG and $\lambda_w=4.0$ cm with an entry taper region of 6 wiggler periods (i.e., $N_w=6$). The electron-beam energy and current is 750 keV and 200 A, respectively, with an initial beam radius

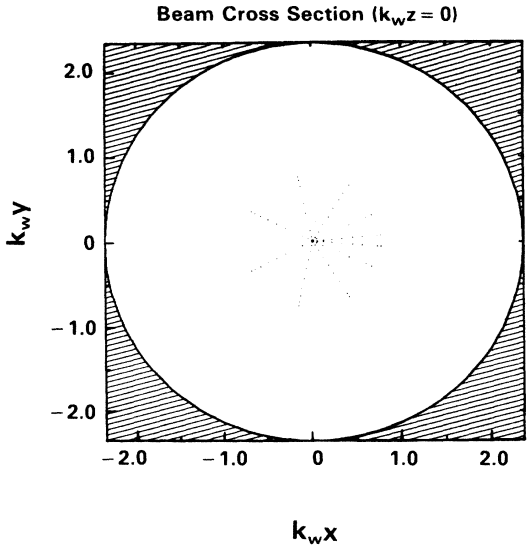

FIG. 4. Plot of the initial electron-beam cross section. The outer circle represents the waveguide wall.

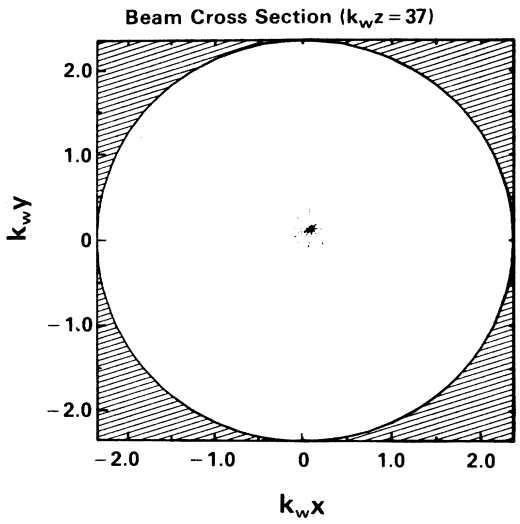

FIG. 5. Electron-beam cross section at the end of the wiggler entry taper region.

of $R_b = 0.5$ cm. Finally, the waveguide radius is $R_g = 1.5$ cm. Before discussing the results with a tapered wiggler, we first consider the interaction for a uniform wiggler field.

The evolution of the radiation power (watts) and growth rate [$\Gamma = d(\ln \delta a_{ln})/dz$] as functions of axial position are shown in Fig. 3 for the $TE_{1,1}$ mode and a frequency of $\omega/ck_w = 8.3$. Input power was chosen to be 10 W and saturation was found at $k_w z = 199$ with a power of 10.9 MW for a total efficiency of $\eta = 7.27\%$. Note that radiation growth was observed over the frequency range $7.7 < \omega/ck_w < 9.3$, and this choice of frequency is for illustrative purposes only. The linear stage of the interaction is seen to occur over the approximate range $70 \lesssim k_w z \lesssim 170$, and the regular oscillation in the growth rate results from a coupling with betatron oscillations in the electron trajectories due to the transverse inhomogeneity in the wigger field. In order to see this, we consider the axial evolution of the beam cross section.

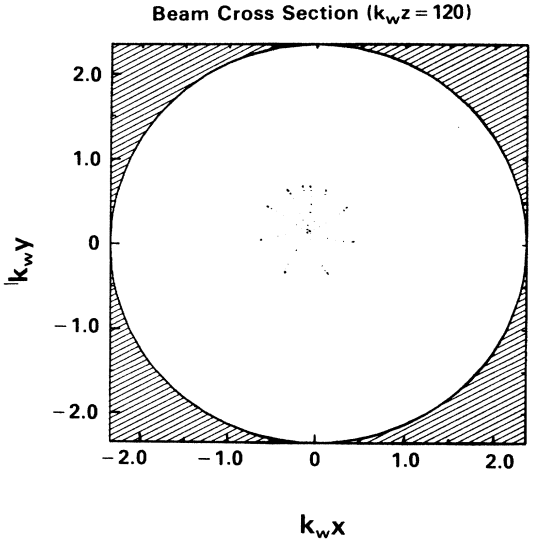

FIG. 6. Electron-beam cross section in the linear phase of the interaction at a local maximum in the growth rate.

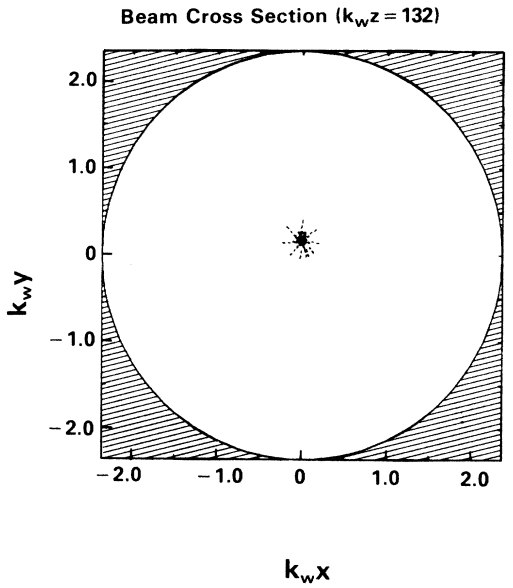

FIG. 7. Electron-beam cross section during the linear phase of the interaction at a local minimum in the growth rate.

The initial beam cross section (i.e., $k_w z = 0$) is shown in Fig. 4, in which the circle represents the waveguide wall and the dots represent a superposition of all the electrons projected onto the transverse x-y plane. Thus, each dot initially represents 10 electrons with a total of 100 dots plotted. The beam cross section at $k_w z = 37$ is shown in Fig. 5, which corresponds to the end of the entry taper region. Three principal effects are evident from these figures. First, the adiabatic increase in the wiggler amplitude has imparted a transverse motion to the electrons, as evidenced by the displacement of the beam center from the axis of symmetry. Second, as shown by the rotation of the two close-set "spokes," the beam is executing a pinwheeling type of motion about the beam center. Third, the beam has been substantially compressed. This

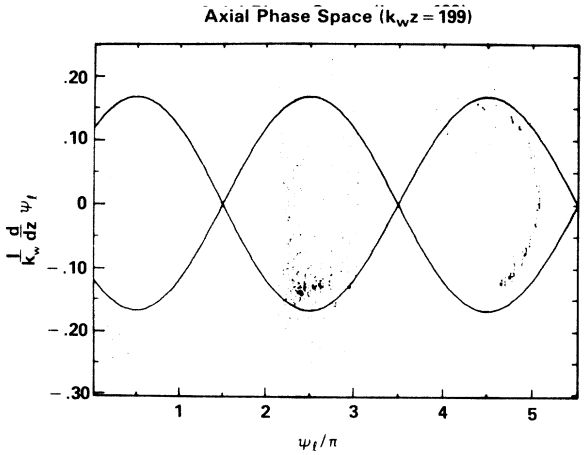

FIG. 8. Axial phase space at saturation. The solid lines represent the separatrices calculated on the basis of the ideal steady-state orbits in a uniform wiggler field.

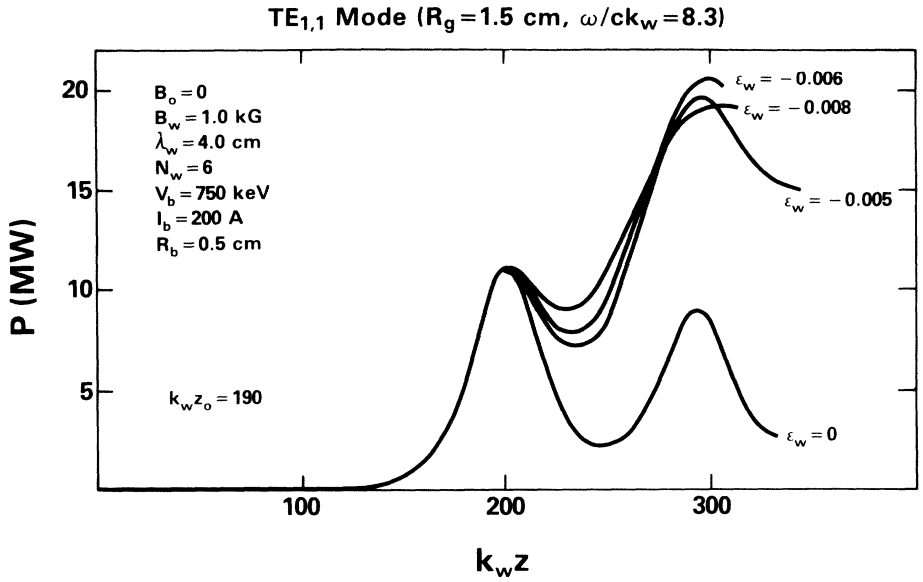

FIG. 9. Radiation power vs axial position for a variety of choices for the wiggler taper in the absence of an axial guide field.

compression of the beam is due, in part, to a focusing effect of the wiggler field, as well as betatron oscillations. The "pinwheeling" of the beam results from the combined effects of the betatron oscillations and a transverse velocity shear across the beam. Subsequent evolution of the beam cross section displays (1) a bulk oscillation of the beam about the axis of symmetry which twists the beam into a helix at the wiggler period, (2) the "pinwheeling" of the beam about its center, and (3) a "scalloping" of the beam cross section due to the betatron oscillation. It is this scalloping of the beam which imparts a modulation to the radiation growth rate. This correlation is shown clearly by comparing the beam cross sections at the local maxima and minima of the growth. In Fig. 6 we show the beam cross section at $k_w z = 120$, which corresponds to a maximum in the growth rate. The beam radius at this point represents a local maximum. The subsequent minimum in the growth rate occurs at $k_w z = 132$, which is displayed by approximately two wiggler periods and one-half of a betatron period. The beam cross section at this point is displayed in Fig. 7, and shows a local minimum in the beam radius.

Finally, saturation occurs at $k_w z = 199$ by means of particle trapping in the ponderomotive potential formed

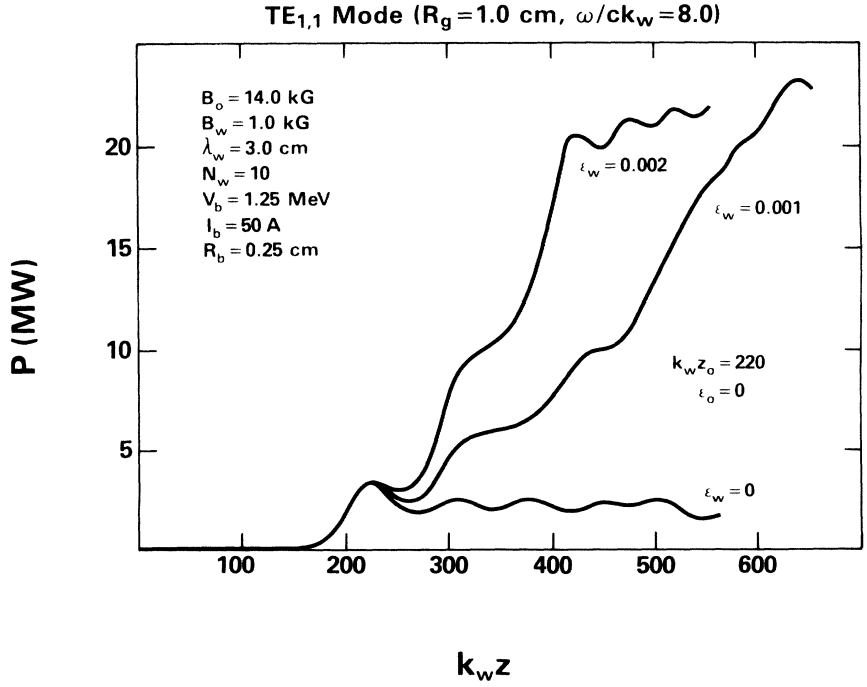

FIG. 10. Radiation power vs axial position for a variety of choices for the wiggler taper. This is the strong axial guide field limit in which $\Phi(\lambda_0) < 0$ for the steady-state orbits.

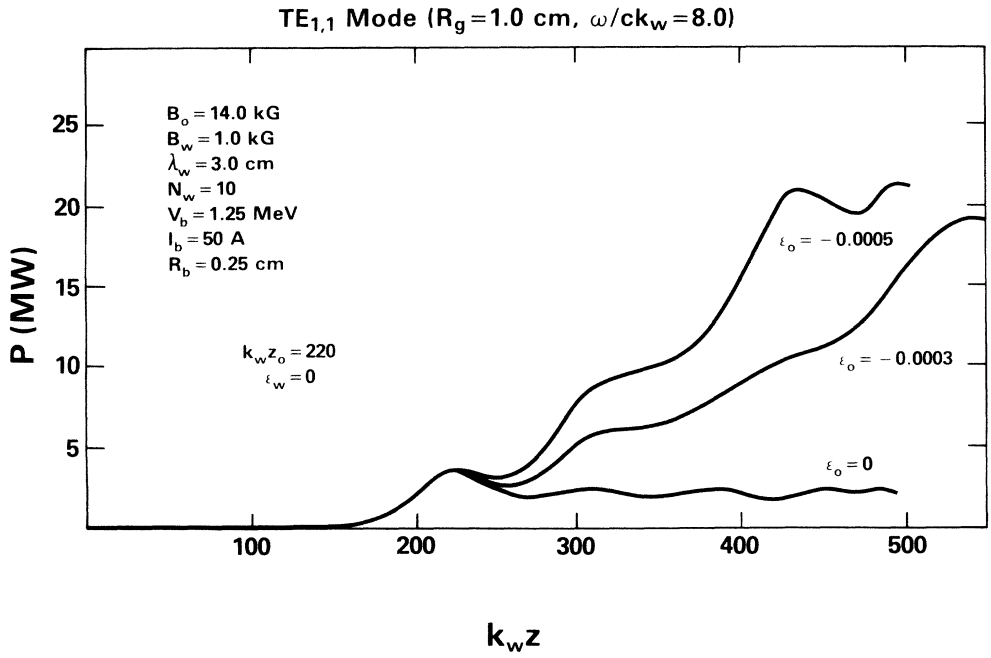

FIG. 11. Radiation power vs axial position for a variety of choices for the axial field taper.

by the beating of the wiggler and radiation fields. This is shown clearly in Fig. 8 where the axial phase space is plotted, and where the solid line represents an approximate separatrix calculated on the basis of the ideal, steady-state trajectories.

The results of simulation runs with a wiggler taper is shown in Fig. 9 for the aforementioned parameters. We plot the power in the radiation mode versus axial position, and include the untapered case for comparison. In general, the efficiency enhancement obtained by means of the tapered wiggler was found to be extremely sensitive to the choice of both the position at which the taper was begun (z_0) and to the slope of the wiggler amplitude (ϵ_w). The optimal results for this choice of parameters are shown in the figure. The maximum efficiency enhancement occurs if the taper is initiated slightly prior to the saturation point of the untapered interaction, which was $k_w z_0 = 190$ for this choice of parameters. In addition, too high a taper was found to be as bad as too low, and the greatest efficiency enhancement ($\eta \simeq 13.7\%$) occurred for $\epsilon_w = -0.006$, which represents an approximate doubling of the efficiency in comparison with the untapered result. Greater enhancements in the efficiency are not possible in this case because the wiggler must be tapered "down," and the results shown have been carried to the point at which the wiggler field and, hence, the interaction vanish.

A series of simulation runs in the presence of an axial guide field has also been carried out for $B_0 = 14$ kG, $B_w = 1$ kG, $\lambda_w = 3$ cm, and $N_w = 10$. The electron-beam parameters used for these runs were $V_b = 1.25$ MeV, $I_b = 50$ A, and $R_b = 0.25$ cm. As before, we consider the $TE_{1,1}$ mode, but the waveguide radius has been decreased to $R_g = 1.0$ cm. Wave amplification in a uniform field structure was found to occur over the frequency range $7.5 \lesssim \omega/ck_w \lesssim 8.5$, and we have chosen $\omega/ck_w = 8.0$ for purposes of illustration. The untapered efficiency in this case was found to be $\eta \simeq 5.61\%$ at $k_w z \simeq 225$. These parameters correspond to group-II trajectories with $\Phi(\lambda_0) < 0$; hence, the wiggler field must be tapered "up" (i.e., $\epsilon_w > 0$) in order to obtain an enhancement in the efficiency. We also observe, from the small-signal theory described in Sec. III, that the resonant enhancement in the untapered gain and efficiency described in the previous literature,[34–37] is mirrored by a resonant enhancement in the effect of tapered fields on the interaction. Thus, in the vicinity of the resonance at $\Omega_0 \simeq \gamma_0 k_w v_{||}$, smaller degrees of taper are required to obtain comparable levels of the resonant phase ψ_{res}. This effect is shown in Fig. 10, in which we plot the radiation power versus axial position for several choices of ϵ_w, and $\epsilon_0 = 0$, (i.e., uniform axial field). Optimal results are found for $k_w z_0 = 220$, and $\epsilon_w = 0.001$. The maximum efficiency in this case was $\eta \simeq 37.1\%$, which is enhanced over the untapered result by almost 700%. Observe that in contrast to the zero-axial-field case, the requirement that $\epsilon_w > 0$ in this regime means that the tapered interaction region can be extended over an indefinite length. This permits larger efficiency enhancements to be achieved. Even so, there appears to be an asymptotic state in which the efficency tapers off as a function of axial length, and only small additional enhancements in the efficiency occur. This is shown in the figure for the choice of $\epsilon_w = 0.002$.

The case of a tapered axial guide field is shown in Fig. 11, in which we plot the radiation power versus axial position for a variety of choices for $\epsilon_0, \epsilon_w = 0$ (uniform wiggler field), $k_w z_0 = 220$, and the same parameters chosen in the generation of Fig. 10. As in the case of the preceding example, these parameters correspond to group-II orbits for which $\Phi(\lambda_0) < 0$. Hence, the axial field must be tapered "down" to achieve an efficiency enhancement. As shown in the figure, optimum efficiency enhancement occurs for $\epsilon_0 = -0.0005$, in which $\eta \simeq 34.5\%$. As in the case of a ta-

pered wiggler field, an asymptotic state is found in which the efficiency enhancement tapers off as a function of axial position. Finally, it should be remarked that the decrease in the axial field implies a divergence of the field lines with axial position. This divergence ultimately results in the loss of the electron beam to the waveguide wall. For the chosen parameters, this loss of the beam to the walls becomes an important consideration for axial field tapers greater than $\epsilon_0 < -0.0005$.

V. SUMMARY AND DISCUSSION

In this paper we have developed a three-dimensional nonlinear theory and numerical simulation of the FEL and ubitron amplifiers with tapered wiggler and axial guide magnetic fields. The model we consider is one in which the field tapering begins close to the saturation point of the untapered interaction, and the results are found to be extremely sensitive to both the starting point and the degree of taper employed. As a result, we conclude that the tapered field configuration required to produce an optimum efficiency enhancement will be a sensitive function of the specific frequency of interest in any given experiment since the saturation length will vary widely over the resonant spectrum.

The axial guide magnetic field is also found to have a profound effect upon the nature of the efficiency enhancement process. The resonant phase (58) is seen to exhibit an enhancement in the regime in which $\Omega_0 \sim \gamma_0 k_w v_{||}$, so that a smaller degree of taper relative to the zero-guide-field limit is required. In addition, the axial field affects the sense of the required taper. In the low-axial-field regime ($\Omega_0 < \gamma_0 k_w v_{||}$) both the wiggler and guide fields must be tapered down in order to obtain an efficiency enhancement. This situation is well known in the literature, and results from the fact that decreases in the wiggler and axial fields cause an axial acceleration of the electron beam which, in turn, preserves the wave-particle resonance. However, the presence of a strong magnetic field ($\Omega_0 > \gamma_0 k_w v_{||}$) results in a markedly different behavior. In particular, when $\Phi(\lambda_0) < 0$ a negative masslike effect occurs in which the electrons are axially accelerated as they lose energy to the wave. As a consequence, the electrons must be decelerated in order to maintain the wave-particle resonance. This is accomplished, in this regime, by an upward taper in the wiggler field and/or a downward taper in the axial guide field. One important consequence of this is that while a "downward" taper in the wiggler field can be maintained only until the wiggler field becomes negligibly small, an "upward" taper can (at least in principle) be maintained over an indefinite interaction length and allow for extremely high levels of efficiency enhancement. Depending upon the specific parameters in any given experiment, this may have an important effect upon the ultimate efficiency achievable.

ACKNOWLEDGMENTS

This work was supported by the U.S. Office of Naval Research. The authors would like to thank Dr. P. Sprangle, Dr. C. M. Tang, and Dr. R. K. Parker for helpful discussions.

*Permanent address: Science Applications International Corp., McLean, VA 22102.

[1]L. R. Elias, W. M. Fairbanks, J. M. J. Madey, H. A. Schwettman, and T. I. Smith, Phys. Rev. Lett. **36**, 717 (1976).

[2]D. A. G. Deacon, L. R. Elias, J. M. J. Madey, G. J. Ramian, H. A. Schwettman, and T. I. Smith, Phys. Rev. Lett. **38**, 892 (1977).

[3]V. L. Granatstein, S. P. Schlesinger, M. Herndon, R. K. Parker, and J. A. Pasour, Appl. Phys. Lett. **30**, 384 (1977).

[4]D. B. McDermott, T. C. Marshall, S. P. Schlesinger, R. K. Parker, and V. L. Granatstein, Phys. Rev. Lett. **41**, 1368 (1978).

[5]R. K. Parker, R. H. Jackson, S. H. Gold, H. P. Freund, V. L. Granatstein, P. C. Efthimion, M. Herndon, and A. K. Kinkead, Phys. Rev. Lett. **48**, 238 (1982).

[6]S. H. Gold, W. M. Black, H. P. Freund, V. L. Granatstein, R. H. Jackson, P. C. Efthimion, and A. K. Kinkead, Phys. Fluids **26**, 2683 (1983).

[7]R. W. Warren, B. E. Newnam, J. G. Winston, W. E. Stein, L. M. Young, and C. A. Brau, IEEE J. Quantum Electron. **QE-19**, 391 (1983).

[8]M. Billandon, P. Elleaume, J. M. Ortega, C. Bazin, M. Bergher, M. Velghe, Y. Petroff, D. A. G. Deacon, K. E. Robinson, and J. M. J. Madey, Phys. Rev. Lett. **51**, 1652 (1983).

[9]J. Edighoffer, G. R. Neil, C. E. Hess, T. I. Smith, S. W. Fornaca, and H. A. Schwettmann, Phys. Rev. Lett. **52**, 344 (1984).

[10]J. Fajans, G. Bekefi, Y. Z. Yin, and B. Lax, Phys. Rev. Lett. **53**, 246 (1984).

[11]S. H. Gold, D. L. Hardesty, A. K. Kinkead, L. R. Barnett, and V. L. Granatstein, Phys. Rev. Lett. **52**, 1218 (1984).

[12]T. J. Orzechowski, B. Anderson, W. M. Fawley, D. Prosnitz, E. T. Scharlemann, S. Yarema, D. Hopkins, A. C. Paul, A. M. Sessler, and J. Wurtele, Phys. Rev. Lett. **54**, 889 (1985).

[13]P. Sprangle, C. M. Tang, and W. Manheimer, Phys. Rev. Lett. **43**, 1932 (1979).

[14]N. M. Kroll, P. L. Morton, and M. N. Rosenbluth, in *Physics of Quantum Electronics: Free-Electron Generators of Coherent Radiation,* edited by S. F. Jacobs, H. S. Piloff, M. Sargent, M. O. Scully, and R. Spitzer (Addison-Wesley, Reading, MA, 1980), Vol. 7, Chaps. 4 and 5, p. 89.

[15]N. M. Kroll and M. N. Rosenbluth, in Ref. 14, Chap. 6, p. 147.

[16]A. Szöke, V. K. Neil, and D. Prosnitz, in Ref. 14, Chap. 7, p. 175.

[17]D. Prosnitz, A. Szöke, and V. K. Neil, in Ref. 14, Chap. 21, p. 571.

[18]S. A. Mani, in Ref. 14, Chap. 22, p. 589.

[19]W. H. Louisell, C. D. Cantrell, and W. A. Wegener, in Ref. 14, Chap. 23, p. 623.

[20]C. A. Brau and R. K. Cooper, in Ref. 14, Chap. 24, p. 647.

[21]P. Sprangle, C. M. Tang, and W. M. Manheimer, Phys. Rev. A **21**, 302, 1980.

[22]C. M. Tang and P. Sprangle, in *Proceedings of the International Conference on Lasers '80,* edited by R. C. Powell (STS Press, McLean, VA, 1980), p. 13.

[23]P. Sprangle and C. M. Tang, Appl. Phys. Lett. **39**, 677 (1981).

[24]J. M. Slater, J. Adamski, D. C. Quimby, W. M. Grossman, T. L. Churchill, and R. E. Center, in *Proceedings of the International Conference on Lasers '82,* edited by R. C. Powell (STS Press, McLean, VA, 1982), p. 212.

[25]H. P. Freund, P. Sprangle, and C. M. Tang, Phys. Rev. A **25**, 3121 (1982).

[26]J. C. Goldstein, in *Free-Electron Generators of Coherent Radiation,* edited by C. A. Brau, S. F. Jacobs, and M. O. Scully [Proc. SPIE **453** (1984)] (SPIE, Bellingham, Washington, 1984), p. 2.

[27]H. P. Freund and S. H. Gold, Phys. Rev. Lett. **52**, 926 (1984).

[28]A. K. Ganguly and H. P. Freund, Phys. Rev. A **32**, 2275 (1985).

[29]L. Friedland, Phys. Fluids **23**, 2376 (1980).

[30]P. Diament, Phys. Rev. A **23**, 2537 (1981).

[31]H. P. Freund and A. T. Drobot, Phys. Fluids **25**, 736 (1982).

[32]H. P. Freund and A. K. Ganguly, IEEE J. Quantum Electron. **QE-21**, 1073 (1985).

[33]H. P. Freund, Phys. Rev. A **27**, 1977 (1983).

[34]L. Friedland and J. L. Hirshfield, Phys. Rev. Lett. **44**, 1456 (1980).

[35]H. P. Freund, P. Sprangle, D. Dillenburg, E. H. da Jornada, R. S. Schneider, and B. Liberman, Phys. Rev. A **26**, 2004 (1982).

[36]L. Friedland and A. Fruchtman, Phys. Rev. A **25**, 2693 (1982).

[37]H. P. Freund and A. K. Ganguly, Phys. Rev. A **28**, 3438 (1983).